

1 Probing key organic substances driving new particle growth initiated by
2 iodine nucleation in coastal atmosphere

3

4 Yibei Wan,¹ Xiangpeng Huang,² Bin Jiang,³ Binyu Kuang,⁴ Manfei Lin,⁴ Deming
5 Xia⁵, Yuhong Liao,³ Jingwen Chen,⁵ Jianzhen Yu,⁴ and Huan Yu¹

6 ¹ Department of Atmospheric Science, School of Environmental Studies, China
7 University of Geosciences, Wuhan, 430074, China

8 ² School of Environmental Science and Engineering, Nanjing University of
9 Information Science and Technology, Nanjing, 210044, China

10 ³ Guangzhou Institute of Geochemistry, Chinese Academy of Sciences, Guangzhou
11 510640, China

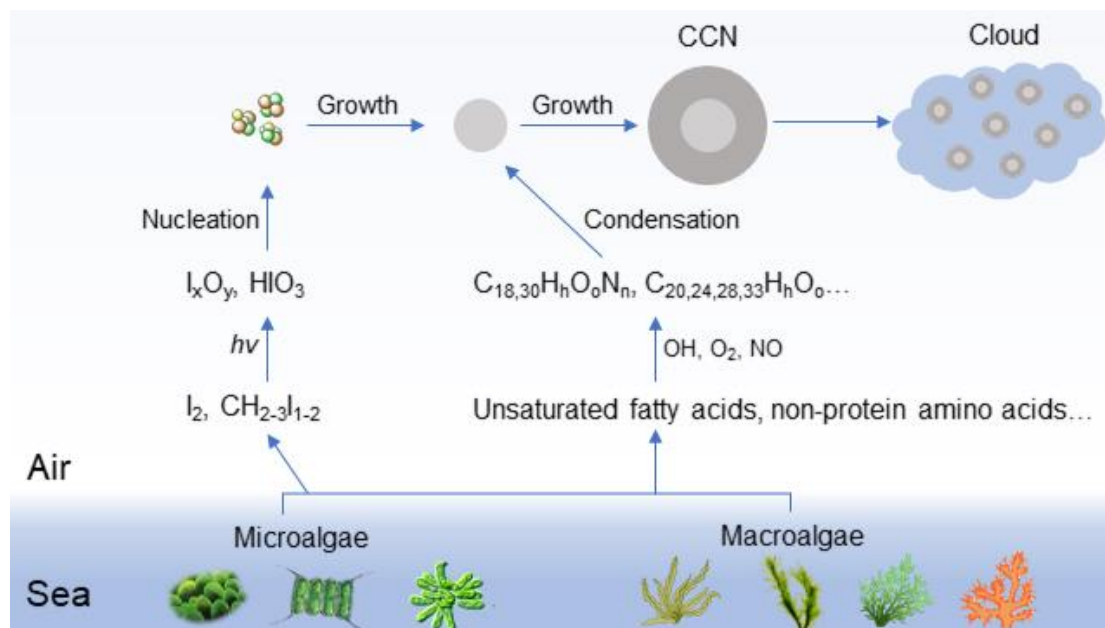
12 ⁴ Department of Chemistry, Hong Kong University of Science & Technology, Clear
13 Water Bay, Kowloon, Hong Kong, China

14 ⁵ School of Environmental Science and Technology, Dalian University of Technology,
15 Dalian 116024, China

16

17 Corresponding author: H. Yu (yuhuan@cug.edu.cn)

18 **Graphic abstract**



19

20 **ABSTRACT**

21 Unlike the deep understanding of highly oxygenated organic molecules (HOMs)
 22 driving continental new particle formation (NPF), little is known about the organic
 23 compounds involved in coastal and open ocean NPF. On the coastline of China we
 24 observed intense coastal NPF events initiated by iodine nucleation, but particle growth
 25 to cloud condensation nuclei (CCN) sizes was dominated by organic compounds. This
 26 article revealed a new group of $C_{18,30}H_nO_oN_n$ and $C_{20,24,28,33}H_nO_o$ compounds with
 27 specific double bond equivalents and oxygen atom numbers in sub-20 nm coastal
 28 iodine new particles by using ultrahigh resolution Fourier transform-ion cyclotron
 29 resonance mass spectrometry (FT-ICR-MS). We proposed these compounds are
 30 oxygenated or nitrated products of long chain unsaturated fatty acids, fatty alcohols,
 31 non-protein amino acids or amino alcohols emitted mutually with iodine from coastal
 32 biota or biological-active sea surface. Group contribution method estimated that the
 33 addition of $-ONO_2$, $-OH$ and $-C=O$ groups to the precursors reduced their volatility of
 34 by 2~7 orders of magnitude and thus made their products condensable onto iodine new
 35 particles in the coastal atmosphere. Non-target MS analysis also provided a list of 440

36 formulas of iodinated organic compounds in size-resolved aerosol samples during the
37 iodine NPF days, which facilitates the understanding of unknown aerosol chemistry of
38 iodine.

39 **1. INTRODUCTION**

40 Atmospheric new particle formation (NPF) contributes over half of global cloud
41 condensation nuclei (CCN) (Merikanto et al., 2009) and thus influences cloud
42 properties and Earth's radiation budget (Metzger et al., 2010). By deploying high
43 resolution Chemical Ionization Mass spectrometer, recent laboratory and field studies
44 have identified a group of highly oxygenated multifunctional organic molecules
45 (HOMs) with high O/C ratios and low volatility from the reactions of volatile organic
46 compounds (VOCs) such as monoterpenes (Ehn et al., 2014), Sesquiterpenes
47 (Richters et al., 2016) and alkene (Mentel et al., 2015) with hydroxyl radical (OH),
48 ozone (O₃), nitrate radicals (NO₃) and chlorine atom (Wang et al., 2020). These
49 HOMs play an important role in particle nucleation and growth of continental NPF, as
50 well as in the formation of secondary organic aerosols.

51 Unlike the deep understanding of continental HOMs, little is known about the role of
52 organic compounds in the NPF in coastal or open ocean atmosphere. The current state
53 of knowledge is that the photolysis of molecular iodine (I₂) or iodomethane is the
54 source of iodine oxides or oxoacids, the self-clustering of which could initiate NPF
55 events with particle number concentration sometimes exceeding 10⁶ cm⁻³ (O'Dowd et
56 al., 2002; Saiz-Lopez and Plane, 2004; Burkholder et al., 2004; Mahajan et al., 2010,
57 2012; Sipilä et al., 2016; Stevanović et al., 2019; Kumar et al., 2018). But it is unknown
58 if other species are needed to drive the growth of iodine clusters to CCN sizes in coastal
59 or open ocean atmosphere (Saiz-Lopez et al., 2012). Iodine-induced NPF (I-NPF)
60 events were mostly reported in European coastlines (Yoon et al., 2006; Mahajan et al.,
61 2010) and polar regions (Allan et al., 2015; Roscoe et al., 2015; Dall'Osto et al., 2018).
62 In 2019 we provided evidences of I-NPF in the southeast coastline of China, based on
63 particle number size distribution and iodine measurements (Yu et al., 2019). The focus

64 of that paper (Yu et al., 2019) is, however, the speciation of organic iodine compounds
65 in size-segregated aerosol samples. Moreover, the use of relatively low resolution
66 Time-of-Flight (TOF) mass analyzer and *in vitro* signal amplification approach in that
67 paper did not allow the detection of the majority of non-aromatic organic iodine
68 compounds. Organic iodine remains to be the most significant unknown in aerosol
69 iodine chemistry at present (Saiz-Lopez et al., 2012).

70 Fourier Transform Ion Cyclotron Resonance (FT-ICR) coupled with soft ionization
71 techniques such as electrospray ionization (ESI) and ambient pressure chemical
72 ionization (APCI) allows characterization of complex organic mixtures at the
73 molecular level due to its ultra-high resolution and mass accuracy (Pratt and Prather,
74 2012). This technique has been used to examine molecular composition of organic
75 aerosols (Schum et al., 2018; An et al., 2019; Zuth et al., 2018; Daellenbach et al., 2018;
76 Xie et al., 2020) and cloud water (Zhao et al., 2013; Bianco et al., 2018). Studies
77 investigating coastal organic aerosols have been rare. Virtually no study reported the
78 characterization of organic compounds driving the growth of coastal or open ocean new
79 particles.

80 In this study, comprehensive chemical composition analyses were conducted on the
81 size-segregated aerosol samples down to 10 nm, collected by 13-stage nano-MOUDI
82 (nano-micro orifice uniform deposit impactor) during the intense I-NPF days at a
83 coastal site of China. Relative abundances of HSO_4^- , total iodine and total organic
84 carbon (TOC) in 10-56 nm particles were compared between the I-NPF days and
85 conventional continental NPF (C-NPF) days. In particular, using ultra-high resolution
86 FT-ICR-MS, we conducted a non-target analysis of particle-phase organic compounds
87 to explore their molecular identity, formation mechanism and the role in new particle
88 growth in the coastal atmosphere.

89 2. METHDOLOGY

90 2.1. Sampling collection

91 The sampling site (29°29' N, 121°46' E) is near a small fishing village without
92 permanent residents in the coastline of East China Sea. It can be seen from the aerial
93 photo (Figure S1a) that from the east to the west are the sea, intertidal zone, small
94 paddy fields and the mountain. The sampling site is about 40 and 200 m away from at
95 high tide and low tide, respectively. The classification of I-NPF event, C-NPF event or
96 non-NPF was based on particle number size distributions (PNSD) between 2 and 750
97 nm monitored from January to May 2018 by a scanning mobility particle spectrometer
98 (SMPS; TSI DMA3081 and CPC3775; scanning range: 40-750 nm) and a neutral
99 cluster air ion spectrometer (NAIS; scanning range: 2-42 nm). A nano-MOUDI
100 sampling scheme was implemented according to the PNSD measurement. One set of
101 nano-MOUDI samples was collected during the C-NPF days from February 11 to 13; a
102 second set was collected during overcast non-NPF days from April 16 to 18; a third set
103 was collected during the I-NPF days from May 9 to 11. The PNSD during the 3 periods
104 are shown in Figure S2. Each set of nano-MOUDI samples was collected continuously
105 for 72 hours, during which NPF occurred on a daily basis, so that particle chemical
106 composition of different event types can be obtained from offline analyses. Aluminum
107 foil filters were used as sampling substrate to avoid the adsorption of gaseous species.
108 For each set of nano-MOUDI samples, two nano-MOUDIs were placed side by side to
109 collect 10-100 nm particles (on stages 10-13; other stages were silicon greased) and 100
110 nm-18 μ m particles (on stages 1-9) separately, in order to reduce potential positive
111 particle-bounce artifacts. Three additional sets of blank samples were collected by
112 placing a high efficiency particulate air (HEPA) filter at the gas inlet of nano-MOUDI.
113 Detailed information on aerosol sample collection could be found in Yu et al. (2019).

114 2.2. Sample preparation and analysis

115 Half of each filter was transferred into a 20 mL tapered plastic centrifuge tube, added
116 10 mL mixed solvent (1:1 v/v water and methanol; LCMS grade). The mixture was
117 sonicated for 40 min and filtered by a 0.2 μm PTFE membrane syringe filter. The
118 filtrate was evaporated to almost dryness in a rotary evaporator below 40 $^{\circ}\text{C}$ and
119 subsequently redissolved in 0.5 mL water. After being centrifuged for 30 min at 12,000
120 rpm, the supernatant was collected for total iodine (I) analysis by Agilent 7500a
121 ICP-MS (Agilent Technologies, Santa Clara, CA, USA) and HSO_4^- analysis by
122 UPLC-ESI-Q-TOF-MS. The measurements of HSO_4^- and total I were elaborated in our
123 previous article Yu et al. 2019. Another half of each filter was extracted in the same
124 way but used for TOC analysis by a TOC analyzer (Model TOC-5000A, Shimadzu,
125 Japan) and non-target MS analysis of organic compounds (OC) by ESI-FT-ICR-MS
126 (Solarix XR 9.4T instrument, Bruker Daltonics, Coventry, UK). Samples were infused
127 by a syringe pump and analyzed in both positive (ESI+) and negative (ESI-) modes.
128 ESI-FT-ICR MS operation conditions are included in Supplement Material. Field blank
129 sample extracts were analyzed following the same procedure.

130

131 2.3. FT-ICR MS data processing

132 A resolving power ($m/\Delta m_{50\%}$) 550,000 at m/z 300 of our FT-ICR-MS allows the
133 determination of possible formulas for singly charged molecular ions. Only m/z values
134 between 150-1000 that satisfies signal/noise (S/N) ratio > 10 were considered. For each
135 m/z value, several scientific rules were applied to calculate a reasonable elemental
136 formula of natural organic molecule: the general formula is $\text{C}_{1-50}\text{H}_{1-100}\text{O}_{0-50}\text{N}_{0-10}\text{I}_{0-3}$ in
137 the ESI+ mode; elemental ratios H/C, O/C, and N/C are limited to 0.3-3, 0-3 and 0-1.3,
138 respectively. The general formula is $\text{C}_{1-50}\text{H}_{1-100}\text{O}_{1-50}\text{N}_{0-5}\text{S}_{0-2}\text{I}_{0-3}$ in the ESI- mode;
139 elemental ratios H/C, O/C, N/C and S/C are limited to 0.3-3, 0-3, 0-0.5 and 0-0.2,
140 respectively. Mass error must be smaller than 0.5 ppm. Formula containing C, H, O, N,
141 S and I isotopologues were removed from the formula lists. A formula with $m/z > 500$

142 was not reported if it did not belong to any CH₂ homologous series. For a formula
143 C_cH_hO_oN_nS_sI_x, double bond equivalents (DBE) defined as $DBE = \frac{2c+2-h+n-x}{2}$ was
144 required to be non-negative. Formula calculation was done following the same
145 procedure for the three field blank samples. All formulas found in the field blank
146 samples, regardless of peak intensity, were excluded from the formula lists of real
147 samples. Aromaticity index (AI) is calculated from $AI = \frac{DBE_{AI}}{C_{AI}} = \frac{1+c-o-s-0.5h}{c-o-s-n}$. If
148 $DBE_{AI} \leq 0$ or $C_{AI} \leq 0$, then $AI = 0$. A threshold value of $AI \geq 0.5$ provides an
149 unambiguous minimum criterion for the presence of aromatic structure in a
150 molecule (Yassine et al., 2014).

151 3. RESULTS AND DISCUSSION

152 3.1. Organic compounds dominate the growth of new particles initiated by iodine 153 nucleation

154 Although our offline technique did not allow us to probe nucleating cluster
155 composition at ~1.7 nm, four facts from our observation support that the NPF events
156 from May 9 to 11 were initiated by iodine nucleation. First, strong I-NPF events were
157 observed almost every sunny day in April and May, which was the growth and farming
158 season of seaweed. HYSPLIT Back-trajectories analysis (Draxler and Rolph, 2010)
159 shows that air masses moved from East China Sea to the sampling site during the
160 I-NPF days from May 8 to 10, 2018 (Figure S1b). Sea breeze was also expected to
161 flow from the sea to the site in the daytime when the I-NPF events occurred. Second,
162 the evolution of PNSD from May 9 to 11 was not like banana-shape C-NPF observed
163 on the winter days, but was markedly similar to prior reports of iodine-nucleation at
164 European coastal sites (Mäkelä et al., 2002; Sipilä et al., 2016). Third, the production of
165 2-7 nm particles (N_{2-7}) during the C-NPFs followed a nearly identical variation with
166 solar radiation (Figure S2c), which is an indication that the C-NPFs was initiated by
167 OH and H₂SO₄ production dictated by solar radiation. However, this was not observed

168 during the I-NPF events, instead, N_{2-7} was anti-correlated to tidal height in the daytime
 169 (Figure S2a). Fourth, probably the most important, mean total I in 10-56 nm particles
 170 during the I-NPF days (13.5 ng m^{-3} , Table 1) was 67 and 36 times higher than those
 171 during the C-NPF days (0.2 ng m^{-3}) and non-event days (0.37 ng m^{-3}). In the same size
 172 range, mean HSO_4^- concentration ($0.2 \text{ } \mu\text{g m}^{-3}$) during the I-NPF days was lower than
 173 that during the C-NPF days ($0.5 \text{ } \mu\text{g m}^{-3}$).

174 By assuming nanometer-sized particles are spherical with a density of 1.5 g cm^{-3} , we
 175 estimate from the PNSD data that aerosol mass in the 10-56 nm size range was
 176 enhanced by 3.0 and $1.3 \text{ } \mu\text{g m}^{-3}$ at most by the selected I-NPF and C-NPF events
 177 (Figure S2b and S2d). The fraction of organic mass (OM) in the aerosol mass can be
 178 further calculated as $(1.5 \times m_{\text{TOC}})/(m_{\text{Total I}} + m_{\text{HSO}_4^-} + 1.5 \times m_{\text{TOC}}) \times 100\%$ by assuming an
 179 OM/TOC ratio of 1.5. The result shows that mass fractions of OM are 95%, 87% and
 180 68%, respectively, in the size bins 10-18 nm, 18-32 nm and 32-56 nm during the I-NPF
 181 days. Therefore, organic compounds dominate the aerosol mass in the 10-56 nm new
 182 particles during the I-NPF days and were critical for I-NPF to contribute to CCN. Our
 183 result is qualitatively consistent with previous measurements showing that nucleation
 184 mode particles initiated by iodine were composed of a remarkable fraction of organic
 185 compounds and sulfate (Mäkelä et al., 2002; Vaattovaara et al., 2006). The main
 186 purpose of this article is to identify these organic compounds during the I-NPF days.
 187 The OC composition during the C-NPF days is beyond the scope of this article.

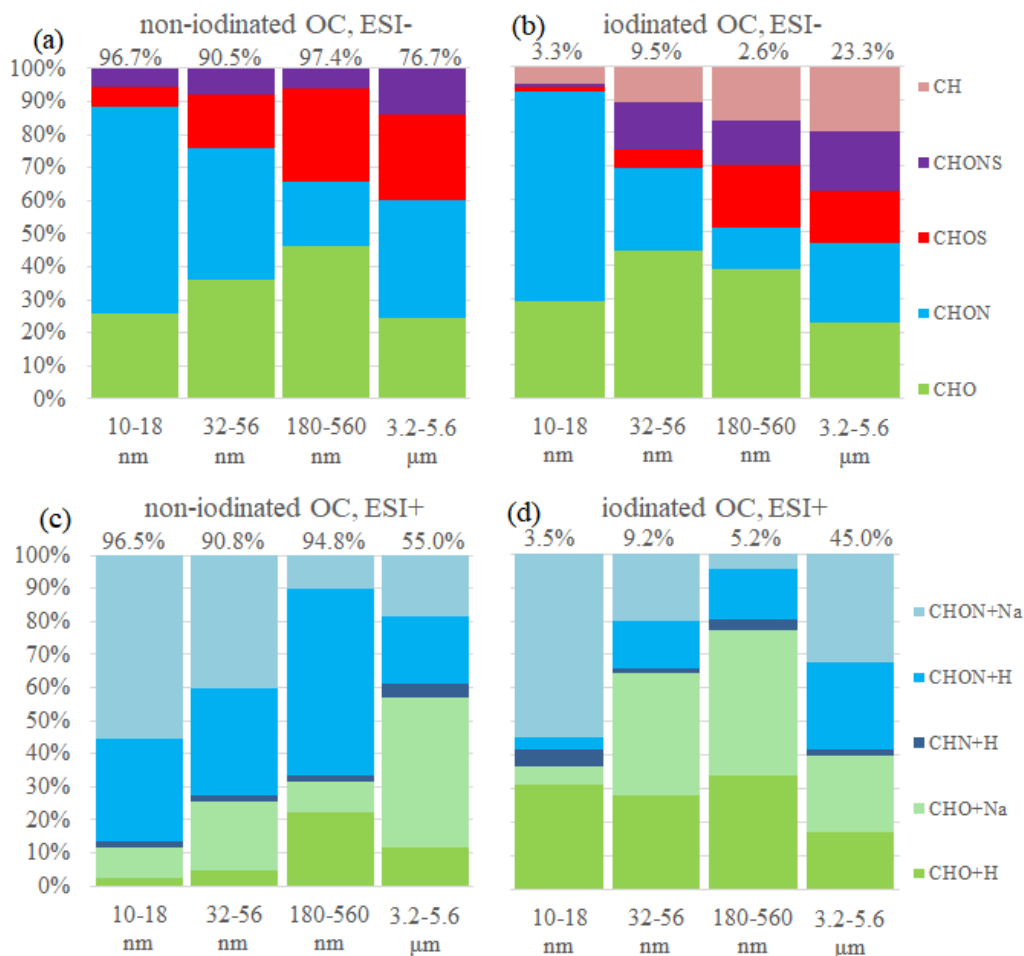
188

189 Table 1. Concentrations of Total iodine (I), HSO_4^- and Total Organic Carbon (TOC) in
 190 3 size bins between 10-56 nm during the I-NPF, C-NPF and non-NPF days. For
 191 simplicity, only the sum of three size bins are shown for the C-NPF and non-NPF days.
 192 BDL=below detection limit.

	I-NPF			C-NPF	non-NPF
	10-18 nm	18-32 nm	32-56 nm	10-56 nm	10-56 nm
Total I ($\mu\text{g m}^{-3}$)	2.3×10^{-3}	6.2×10^{-3}	5.0×10^{-3}	0.20×10^{-3}	0.37×10^{-3}
HSO_4^- ($\mu\text{g m}^{-3}$)	2.2×10^{-2}	3.4×10^{-2}	14.4×10^{-2}	50×10^{-2}	BDL
TOC ($\mu\text{g m}^{-3}$)	3.1×10^{-1}	1.8×10^{-1}	2.1×10^{-1}	2.8×10^{-1}	BDL

193 **3.2. Elemental composition of non-iodinated OC on the I-NPF days**

194 Non-target analysis of OC elemental composition was performed in detail on 10-18
 195 nm, 32-56 nm, 180-560 nm and 3.2-5.6 μm particles during the I-NPF days. Elemental
 196 formulas in the 4 size bins can represent OC molecular composition of nucleation mode,
 197 Aitken mode, accumulation mode and coarse mode, respectively. OC formulas were
 198 divided into two categories: non-iodinated OC and iodinated OC. There are far more
 199 non-iodinated OC formulas than iodinated OC formulas in $<1 \mu\text{m}$ particles in terms of
 200 both formula number (Table 2) and relative intensity (Figure 1). For example, 2831
 201 non-iodinated OC formulas account for 96.6% of OC total intensity in 10-18 nm
 202 particles, while 137 iodinated OC formulas account for the remaining 3.4%. It means
 203 that non-iodinated OC dominates new particle growth during the I-NPF events. In this
 204 section, we first discuss chemical characteristics of non-iodinated OC, while the
 205 speciation of iodinated OC will be discussed in Section 3.4.



206

207 Figure 1. Relative intensity distributions of elemental groups observed in 10-18 nm,
 208 32-56 nm, 180-560 nm and 3.2-5.6 μm size bins in ESI+ and ESI- modes. The
 209 percentage above a column denote the percent of non-iodinated OC (or iodinated OC)
 210 intensity in total OC intensity in a size bin. +Na and +H denote $[\text{M}+\text{Na}]^+$ and $[\text{M}+\text{H}]^+$
 211 adduct in ESI+ mode, respectively.

212 The molecular formulas of non-iodinated OC were divided into seven elemental
 213 groups CHO^- , CHO^+ , CHON^- , CHON^+ , CHOS^- , CHONS^- and CHN^+ . The number
 214 distribution of 7 elemental groups for the 4 size bins is listed in Table 2. If both
 215 $[\text{M}+\text{Na}]^+$ and $[\text{M}+\text{H}]^+$ adducts of a formula were detected, the formula was counted
 216 only once. It should be noted that some formulas were repeatedly detected in ESI+ and
 217 ESI- modes. Some formulas detected in one size bin were also detected in another size
 218 bin. This is quantitatively shown in the first four rows of Table 2. For instance, 58%, 25%
 219 and 4% of the formulas detected in 10-18 nm aerosols were also detected in 32-56 nm,
 220 180-560 nm and 3.2-5.6 μm aerosols, respectively. In another word, the particles in
 221 neighboring size bins share more similarity in organic composition. An unexpected
 222 finding is that the number of non-iodinated OC formulas detected in 3.2-5.6 μm
 223 coarse particles ($n = 266$) is one order of magnitude lower than those of other bins.
 224 Reconstructed mass spectra of the 7 elemental groups in ESI- and ESI+ modes are
 225 shown in Figure S3 for the four size bins.

226

227 Table 2. The numbers of assigned formulas of elemental groups of organic compounds
 228 in 10-18 nm, 32-56 nm, 180-560 nm and 3.2-5.6 μm size bins. The first 4 rows show the
 229 percent of formula repeatability between two size bins. 1I-OC: molecular formula
 230 containing one iodine atom.

Repeatability	10-18 nm	32-56 nm	180-560 nm	3.2-5.6 μm	
10-18 nm		58%	25%	4%	
32-56 nm	57%		38%	4%	
180-560 nm	34%	51%		6%	
3.2-5.6 μm	35%	35%	34%		
Non-iodinated OC					Total
CHO^-	531	565	525	20	892
CHO^+	250	501	380	111	857

CHON ⁻	1005	638	347	25	1268	
CHON ⁺	1139	1055	828	72	2121	
CHOS ⁻	147	216	256	22	357	
CHONS ⁻	134	131	93	10	259	
CHN ⁺	34	26	7	7	46	
Total	2831	2770	2151	266	4979	
Iodinated OC						Total II-OC (%)
CHOI ⁻	32	53	11	5	80	64%
CHOI ⁺	17	85	31	31	136	93%
CHONI ⁻	52	29	7	7	77	88%
CHONI ⁺	34	57	18	52	132	81%
CHOSI ⁻	3	8	7	3	18	72%
CHONSI ⁻	2	7	3	2	13	62%
CHNI ⁺	6	4	4	3	16	56%
CHI ⁻	4	2	1	4	9	67%
Total	137	228	76	100	440	80%

231 CHON is the most commonly assigned elemental group in both ESI+ (2121
232 CHON⁺) and ESI- (1268 CHON⁻) modes, followed by the CHO group (857 CHO⁺
233 formulas and 892 CHO⁻ formulas). S-containing formulas are 357 CHOS⁻ and 259
234 CHONS⁻. The formula number of the least common CHN⁺ group is only 46. In terms
235 of relative intensity, CHON fraction in the ESI- mode decreases from 61% of OC in
236 the 10-18 nm bin to 20% in the 180-560 nm bin (Figure 1a), while the fractions of
237 CHO and CHOS/CHONS increase with particle size. In the ESI+ mode, the fraction of
238 CHON decreases from 88% in 10-18 nm bin to 70% in 180-560 nm bin, being always
239 the dominant elemental group of non-iodinated OC (Figure 1b). Low molecular
240 weight (LMW) amines are important stabilizers in acid-base nucleation (Kurtín et al.,
241 2008; Jen et al., 2014; Zheng et al., 2000; Yao et al., 2016), but their molecular ions
242 are out of the mass range of our FT-ICR-MS. The CHN⁺ formulas that we observed
243 contained 9-50 C atoms and 1-7 N atoms, accounting for a negligible fraction 1.7%
244 of total intensity of all ESI+ formulas in the 10-18 nm particles.

245 Previous elemental composition studies using FT-ICR-MS were mostly conducted
246 on PM_{2.5} or PM₁₀ collected from marine (Schmitt-Kopplin et al., 2012; Bao et al., 2018;
247 Ning et al., 2019), urban (Wu et al., 2019; Jiang et al., 2016), free troposphere (Schum
248 et al., 2018; Mazzoleni et al., 2012) and forest sites (Kourtchev et al., 2013). In general,
249 these studies showed that the numbers of CHO compounds were comparable with or

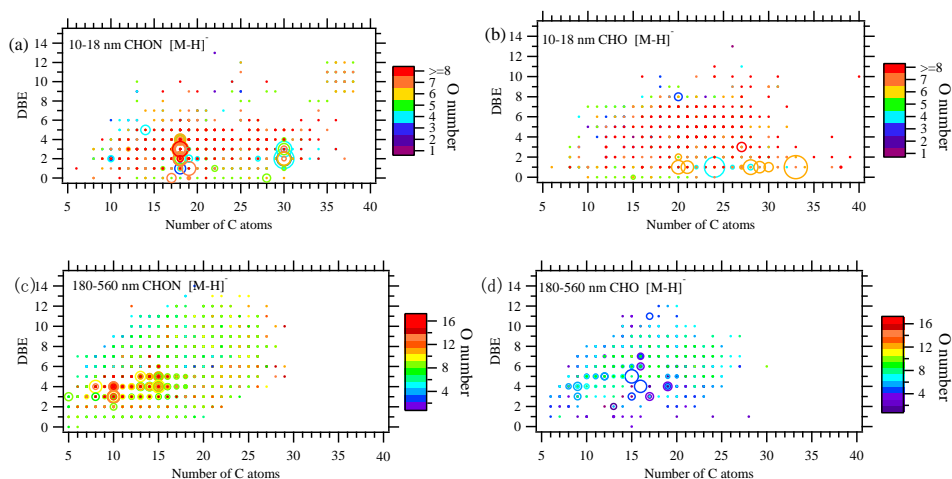
250 more than those of CHON compounds. Our study shows clearly that elemental
251 composition of aerosol OC is highly size dependent. New particle growth in the size
252 range of 10-18 nm during the I-NPF event is dominated by CHON elemental group,
253 followed by CHO. The focus of this article narrows on the identity and source of the
254 CHON and CHO formulas in 10-18 nm particles, by comparing with those in the
255 180-560 nm size bin.

256

257 3.2.1. CHO formulas

258 There is a total of 531 CHO⁻ formulas and 250 CHO⁺ formulas in 10-18 nm
259 particles. 54 CHO formulas are commonly found in ESI⁺ and ESI⁻ modes. In terms
260 of relative intensity, CHO⁻ compounds are more abundant than CHO⁺ compounds
261 (Figure 3b, total intensity: 4.14×10^9 vs. 1.24×10^9). However, this is not indicative of
262 absolute concentration of the two groups due to different ionization efficiency
263 between ESI⁻ and ESI⁺ modes. CHO⁻ is characterized by a series of formulas with 20,
264 24, 28, and 33 C atoms, 4 or 6 O atoms and 1 equivalent double bond (Figure 2b). The
265 total intensity of top 10 formulas accounts for 30% of all 531 formulas. Assuming
266 CHO⁻ formulas contain at least 1 carboxylic group (-COOH), the rest of their
267 molecules should be saturated (DBE = 0) and contain 2 or 4 O atoms.

268



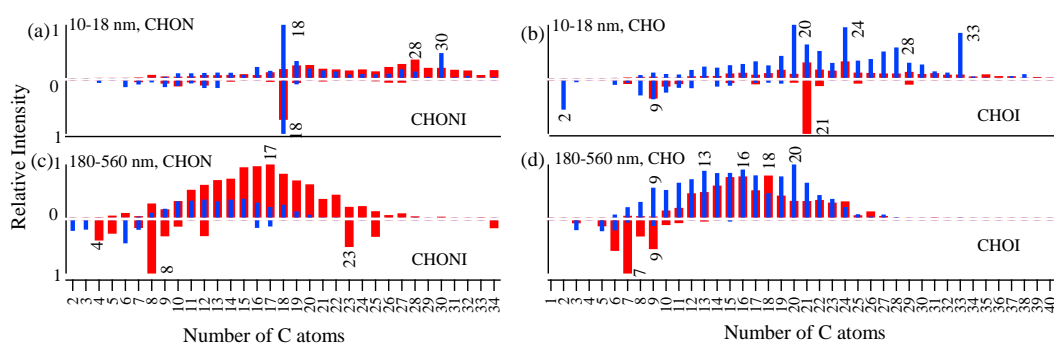
269

270 Figure 2. DBE vs. C atom number diagrams of all CHON and CHO formulas detected
271 in 10-18 nm and 180-560 nm particles in ESI⁻ mode. The color bar denotes O atom

272 number in the formulas. The size of the circles reflects the relative intensities of
273 molecular formulas on a logarithmic scale.

274

275 The above feature is not seen in either CHO⁺ formulas in the 10-18 nm bin or CHO⁻
276 formulas in the 180-560 nm bin. There are more C₂₁ and C₂₄ formulas than other C
277 subgroups in the CHO⁺ formulas of 10-18 nm bin (Figure S4d), but none of them have
278 exceptionally-high intensity. The prominent formulas in the CHO⁻ group in 180-560
279 nm particles have a relatively high unsaturation degree (DBE = 3-7, Figure 2d). The
280 relative intensities of subgroups according to C atom number in the CHO⁻ formulas in
281 the 180-560 nm bin are characterized by trimodal distribution with maximum intensity
282 around C₉, C₁₃-C₁₆ and C₂₀ (Figure 3d). The relative intensity of O atom subgroups is
283 mono-modally distributed around O₇ (Figure S5).



284

285 Figure 3. Relative intensities of subgroups according to C atom number in CHON,
286 CHO, CHONI and CHOI formulas in 10-18 nm and 180-560 nm particles in ESI+ (in
287 red) and ESI- (in blue). The intensity of the most abundant subgroup in a size bin is
288 defined as 1 and those of other subgroups are normalized by it. The relative intensities
289 of non-iodinated OC formulas (iodinated OC formulas) are plotted in the region above
290 (below) zero line.

291

292 3.2.2. CHON formulas

293 As discussed earlier, CHON is the most abundant elemental group observed in the
294 smallest size bin 10-18 nm. There is a total of 1005 CHON⁻ formulas (total intensity
295 9.96×10^9) and 1139 CHON⁺ formulas (6.45×10^9) in 10-18 nm bin. 355 CHON

296 formulas are commonly found in ESI+ and ESI- modes. A close examination of Figure
297 2a and 3a reveals that CHON^- is characterized by a series of C_{18} and C_{30} formulas with
298 low DBE values (1-4). 87 C_{18} and 26 C_{30} formulas account for 37% of total intensity of
299 CHON^- . Such feature is not seen for CHON^+ formulas that are rather uniformly
300 distributed in DBE vs. C diagram (Figure S4a and S4c). Generally speaking, CHON^-
301 compounds should contain nitro- ($-\text{NO}_2$) or nitrooxy- ($-\text{ONO}_2$) group and are
302 ionizable due to the presence of $-\text{COOH}$ or hydroxy ($-\text{OH}$) (Lin et al., 2012). However,
303 the presence of amine group in CHON^- formulas cannot be excluded. Take C_{18} as
304 example, 51 out of 87 $\text{C}_{18}\text{H}_h\text{O}_o\text{N}_n^-$ formulas should contain at least one amine group,
305 either because their O atom numbers are not large enough to allow the assignment of $-\text{NO}_2$
306 for all N atoms, or because some formulas (25 out of 87) were also detected in
307 ESI+ mode. In total, 51 $\text{C}_{18}\text{H}_h\text{O}_o\text{N}_n^-$ formulas with an amine group account for 54.4%
308 of total intensity of 87 $\text{C}_{18}\text{H}_h\text{O}_o\text{N}_n^-$ formulas.

309 The presence of amine group in $\text{C}_{18}\text{H}_h\text{O}_o\text{N}_n^-$ formulas in 10-18 nm particles is also
310 supported by the comparison with CHON^- in 180-560 nm submicron aerosols. CHON^-
311 in 180-560 nm is characterized by a number of formulas with maximum intensity
312 around C_{10} and C_{15} (Figure 2c). A plot of O atom number vs. N atom number in Figure
313 S6a shows that $\text{C}_{10}\text{H}_h\text{O}_o\text{N}_n^-$ in 180-560 nm have O/N ratios ≥ 3 and O atom number is
314 positively correlated with N atom number. It indicates that these $\text{C}_{10}\text{H}_h\text{O}_o\text{N}_n^-$ formulas
315 are probably nitro- or nitrooxy- oxidation products of monoterpenes from continental
316 plant emission. In contrast, O/N ratios of the $\text{C}_{18}\text{H}_h\text{O}_o\text{N}_n^-$ formulas in 10-18 nm are
317 mostly small and O atom number do not increase with N atom number (Figure S6b). All
318 collective evidences above reveal that nitrogen-containing organic compounds in 10-18
319 nm particles during the I-NPF days are partly composed of long-chain amino alcohols,
320 amino acids and so on.

321 In summary, a series of very distinctive CHON^- and CHO^- formulas was observed
322 in 10-18 nm new particles during the I-NPF days. These formulas are characterized by
323 some specific numbers of C atoms (i.e. $\text{C}_{18}\text{H}_h\text{O}_o\text{N}_n$, $\text{C}_{30}\text{H}_h\text{O}_o\text{N}_n$, $\text{C}_{20}\text{H}_h\text{O}_o$, $\text{C}_{24}\text{H}_h\text{O}_o$,
324 $\text{C}_{28}\text{H}_h\text{O}_o$ and $\text{C}_{33}\text{H}_h\text{O}_o$) and equivalent double bonds (DBE = 1 for CHO^- and 1-4 for
325 CHON^-). Monomer-dimer distribution pattern that can arise from particle-phase

326 oligomerisation (Pospisilova et al., 2020) was not observed for these formulas in the
327 mass spectra. We also assume that $C_{18,30}H_hO_oN_n$ and $C_{20,24,28,33}H_hO_o$ are not labile
328 intermediates like ester hydroperoxides that may undergo fast decomposition in the
329 particles or during the sample preparation process (Zhao et al. 2018 a,b). To the best
330 of our knowledge, such $CHON^-$ and CHO^- formulas have not been reported by
331 previous aerosol studies. The chemical composition of new particles is completely
332 decoupled with the CHO^- and $CHON^-$ formulas around C_{10} , C_{15} and C_{20} in 180-560
333 nm submicron particles, which might be originated from continental terpene
334 emissions. Fewer O atoms in $C_{18,30}H_hO_oN_n$ and $C_{20,24,28,33}H_hO_o$ formulas than those in
335 submicron aerosols indicate that these compounds should be more freshly emitted into
336 the atmosphere. The discontinuous chemical composition and PNSD spectrum
337 (Figure S2b) below and above 50 nm particle size reflect the fact that the further
338 growth of new particles beyond 50 nm in local I-NPF events cannot be monitored by
339 our stationary sampling strategy.

340 On the other hand, we observed more complicated distributions of CHO^+ and
341 $CHON^+$ formulas in 10-18 nm new particles that are of relatively small individual
342 intensity and are rather uniformly distributed in DBE vs. C diagrams. Like $CHON^-$
343 and CHO^- , those CHO^+ and $CHON^+$ formulas also possess a larger number of C
344 atoms ($C > 19$) than their counterparts in 180-560 nm submicron aerosols (Figure 3).
345 21 out of 30 most abundant $CHON^+$ formulas contain two or more N atoms; this ratio
346 21/30 is higher than those in $CHON^-$ formulas. Generally speaking, CHO^+ and
347 $CHON^+$ formulas represent carbonyls/alcohols/epoxides and amino alcohols/amino
348 acids, respectively. One interesting finding about CHO^+ and $CHON^+$ is that they
349 tend to form $[M+Na]^+$ adducts in small aerosols and $[M+H]^+$ adducts in large
350 aerosols (Figure 1c). This indicates that the CHO^+ and $CHON^+$ compounds in new
351 particles during the I-NPF days should possess different basic functional groups
352 from those in submicron particles.

353 **3.3. Possible precursors and formation mechanism of organic compounds**

354 **detected in 10-18 nm new particles during the I-NPF days**

355 It is unrealistic to simply propose one out of a large number of possible structures
356 for a formula with large C atom number (e.g., ≥ 18). Our strategy is to first explore
357 the possible precursors of the newly found $C_{18,30}H_nO_n$ and $C_{20,24,28,33}H_nO_n$
358 formulas. Obviously, $C_{18,30}H_nO_n$ and $C_{20,24,28,33}H_nO_n$ formulas cannot be attributed
359 to continental terpene emission or anthropogenic aromatic emissions. Sporadic
360 spikes of 10-18 nm particles that can be an indication of cooking and traffic
361 emissions were not seen in the PNSD spectrum, because such human activities were
362 rare around the site during the sampling period. We thus also exclude the possibility
363 of cooking and traffic emissions.

364 Previous field measurements of marine NPF precursor focused on volatile species
365 like iodine (Stevanović et al., 2019), iodomethanes (O'Dowd et al., 2002), dimethyl
366 sulfonic acid (Yvon et al., 1996; Barone et al., 1996; Barnes et al., 2006) and LMW
367 amines (Ning et al., 2019; Ge et al., 2011). So far there is no report about aliphatic
368 compounds with C number ≥ 18 in either gas phase or new particles (Cochran et al.,
369 2017; Bikkina et al., 2019). Therefore, we consulted the literature that reported
370 chemical compounds isolated from biological tissues of algae, plankton or other
371 marine organisms. Potential precursors are listed in Table 3.

372 **3.3.1. Fatty acids**

373 Fatty acids (FAs) are widely found in animals, plants and microbe (Moss et al.,
374 1995). Plants have higher content of unsaturated FAs than animals. C_{14} - C_{24} fatty acids,
375 including both saturated and unsaturated, have long been observed in seaweed
376 (Dawczynski et al., 2007). Very long chain FAs (C_{24} - C_{36}) have been isolated from
377 green algae, *Chlorella kessleri*, sponges and marine dinoflagellate (Litchfield et al.,
378 1976; Řezanka and Podojil, 1984; Mansour et al., 1999). C_{18} Oleic acid, linoleic acid
379 and linolenic acid are most commonly found unsaturated FAs in macro algae. FAs
380 with carbon chain shorter than C_{20} were used by atmospheric chemists as organic

381 tracers of atmospheric aerosols from microbe or kitchen emission (Simoneit and
 382 Mazurek, 1982; Zheng et al., 2000; Guo et al., 2003; Rogge et al., 1991; DeMott et al.,
 383 2018; Willoughby et al., 2016). In our study, no saturated FAs were detected in 10-18
 384 nm particles. Only 1.5% of CHO⁻ formulas can be assigned to unsaturated FAs (that
 385 is, include 2 O atoms, 14-28 C atoms and DBE = 3-6). Other CHO compounds
 386 observed in 10-18 nm particles contain > 2 O atoms and thus can be assigned as the
 387 oxidized derivatives of FAs.

388

389 Table 3 Possible precursors and their presence in marine biological sources and our
 390 aerosol samples. ND: not detected.

	Potential precursors	Presence in marine sources	Presence in aerosol particles
Unsaturated fatty acid	C ₁₄ -C ₂₄ fatty acids	Seaweed (Dawczynski et al., 2007)	1.5% of CHO ⁻ in terms of relative intensity
	C ₂₅ --C ₃₆ very long chain fatty acids	Green algae, chlorella kessleri, sponges, marine dinoflagellate (Litchfield et al., 1976; Řezanka and Podojil, 1984; Mansour et al., 1999).	ND
fatty alcohols	C ₃₀ -C ₃₂ mono- and diunsaturated alcohols and diols	Yellow-green algae (Volkman et al., 1992)(eustigmatophytes)	ND
Saturated hydroxyl fatty acids	C ₂₀ H ₄₀ O ₃ , C ₃₂ H ₆₄ O ₄	Nannochloropsis, cutins and suberins of higher plants (Gelin et al., 1997).	S/N 15 and 28
Nonprotein amino acid	C ₁₈ H ₃₇ NO ₄ saturated dihydroxy amino acid (simplifungin,		S/N 280
	C ₂₀₋₂₂ H ₃₉₋₄₁ NO ₅₋₇ mono-unsaturated polyhydroxy amino acids in sphingolipids	Marine fungal metabolites (Ishijima et al., 2016; VanMiddlesworth et al., 1992).	S/N 30-230
Amino alcohols	C ₁₆₋₂₈ H ₃₃₋₅₃ NO ₁₋₄ polyhydroxy amino alcohols	Plant biomembrane, secondary metabolites in marine organisms (Jares-Erijman et al., 1993).	S/N 23-640
	C ₁₈ H ₃₁ NO and C ₁₈ H ₂₉ NO polyunsaturated amino alcohols	Mediterranean tunicate (Jares-Erijman et al., 1993)	S/N 10-60
	C ₁₈ H ₃₆ N ₂ O ₅ polyhydroxy cyclic alkaloid	Moraceae (Tsukamoto et al., 2001)	S/N 800

391

392 Possible oxidation schemes of two typical C₁₈ (C₁₈H₃₀O₂, α-linolenic acid, three
 393 C=C double bonds in carbon chain) and C₂₈ unsaturated FAs (C₂₈H₅₂O₂, two C=C
 394 double bonds), for instance, are proposed in Figure S7 and S8. The reaction of an
 395 unsaturated FA after the emission into the atmosphere is initiated by OH addition to
 396 C=C double bond and subsequent O₂ addition to form a peroxy radical (Atkinson et

397 al., 1995; Calvert et al., 2000). Depending on the level of NO and reactivity, four
398 competitive pathways are available for peroxy radicals to produce CHO or CHON
399 formulas observed in our study: reaction with NO to form a $-\text{ONO}_2$ group (pathway
400 1) or an alkoxy radical that further reacts with O_2 to form a carbonyl ($-\text{C}=\text{O}$, pathway
401 2), reaction with RO_2 radicals to form a hydroxyl ($-\text{OH}$) or a $-\text{C}=\text{O}$ group (pathway 3)
402 and successive intermolecular H-shift/ O_2 addition autoxidation (Crouse et al., 2013;
403 Vereecken et al., 2015) (pathway 4).

404 Pathways 1 and 2 add $-\text{ONO}_2$, $-\text{OH}$ and $-\text{C}=\text{O}$ groups to carbon chain but do not
405 reduce the DBE of FA precursor. We propose that pathway 1 and 2 are preferred for
406 those FAs with higher reactivity with NO (e.g., α -linolenic acid, Figure S7).
407 α -linolenic acid oxidation in the atmosphere via sequential occurrences of pathways 1
408 or 2 yields a series of oxygenated and nitrated organic compounds, among which
409 $\text{C}_{18}\text{H}_{31}\text{NO}_6$, $\text{C}_{18}\text{H}_{31}\text{NO}_8$, $\text{C}_{18}\text{H}_{31}\text{NO}_{10}$, $\text{C}_{18}\text{H}_{32}\text{N}_2\text{O}_{10}$ and $\text{C}_{18}\text{H}_{33}\text{N}_3\text{O}_4$ are found in
410 10-18 nm particles. These formulas explain the circles with DBE = 4 and C number =
411 18 shown in Figure 2a (DBE vs. C atom number diagram).

412 The net outcome of sequential pathway 3 and 4 reactions is to add $-\text{OH}$ and $-\text{C}=\text{O}$
413 groups and reduce the DBE of FA precursor. We propose that pathway 3 and 4 are
414 preferred for those FAs (e.g. C_{28} FA $\text{C}_{28}\text{H}_{52}\text{O}_2$) with higher reactivity with RO_2
415 (Figure S8). The end products are a series of $\text{C}_{28}\text{H}_{52}\text{O}_{6-8}$, $\text{C}_{28}\text{H}_{54}\text{O}_{4-7}$ and $\text{C}_{28}\text{H}_{56}\text{O}_{6-8}$
416 compounds, which can explain the circles with C number = 28 and DBE = 1-3 in
417 Figure 2b.

418 In addition to fatty acids, fatty alcohols such as C_{30} - C_{32} mono- and di-unsaturated
419 alcohols and diols have been detected in yellow-green algae (Volkman et al., 1992).
420 Although these unsaturated alcohols were not detected in our 10-18 nm particles, we
421 suppose that they or their metabolites in algae may undergo similar reactions like
422 unsaturated FA to generate condensable oxygenated and nitrated fatty alcohols in the
423 atmosphere. Hydroxy fatty acids (HFAs) are important constituents of lipid in
424 marine microalgae (Gelin et al., 1997), bacteria (Kim and Oh, 2013), seaweed
425 (Kendel et al., 2013; Blokker et al., 1998) and leaf surface of higher plants (Pollard
426 et al., 2008). Among them, two saturated HFAs $\text{C}_{20}\text{H}_{40}\text{O}_3$ and $\text{C}_{32}\text{H}_{64}\text{O}_4$ were found

427 in our 10-18 nm aerosol sample with S/N ratios 15 and 28. However, because
428 saturated hydroxy fatty acids are not oxidizable via the pathways proposed in our
429 study, they are assumed unlikely to be precursors of other formulas observed in
430 10-18 nm particles.

431 3.3.2. *Nonprotein amino acids and amino alcohols*

432 Quantum chemical calculations have showed that amino acids like Glycine, Serine,
433 and Threonine are potential participants in atmospheric nucleation via interaction
434 with sulfuric acid (Elm et al., 2013; Ge et al., 2018; Li et al., 2020). However, we
435 did not observe any of 20 essential amino acids in 10-18 nm in either ESI+ or ESI-
436 modes. One reason may be that most of essential amino acids have molecular weight
437 less than 150 that is below mass scan range of our FT-ICR-MS.

438 There are a number of records in the literature about long chain non-protein amino
439 acids or amino alcohols isolated from marine organisms or plant biomembrane
440 (Ishijima et al., 2016; VanMiddlesworth et al., 1992; Jares-Erijman et al., 1993;
441 Tsukamoto et al., 2001). They include saturated dihydroxy amino acid ($C_{18}H_{37}NO_4$,
442 DBE = 1, simplifungin), monounsaturated polyhydroxy amino acids in sphingolipids
443 ($C_{20-22}H_{39-41}NO_{5-7}$, DBE = 2-3), polyhydroxy amino alcohols ($C_{16-28}H_{33-53}N_{1-2}O_{1-5}$,
444 DBE = 1-3, sphingosine and its natural metabolites) and polyunsaturated amino
445 alcohols ($C_{18}H_{31}NO$ and $C_{18}H_{29}NO$, DBE = 4-5). All of these formulas were detected
446 in 10-18 nm aerosols with S/N in the range of 10-800. More importantly, all those
447 compounds that contain at least one amine group and one C=C double bond can be
448 precursors of observed CHON formulas containing amine group via the pathways that
449 we showed above. As an example, the oxidation scheme of an amino alcohol
450 $C_{18}H_{31}NO$ with 4 C=C double bonds in carbon chain is illustrated in Figure S9.

451 Similar to C_{28} FA, $C_{18}H_{31}NO$ undergoes successive intermolecular H-shift/ O_2
452 additions to produce a series of RO_2 radicals with hydroperoxyl group ($-OOH$) in its
453 carbon chain. The subsequent pathway 3 reactions, as well as the decomposition of $-$
454 OOH groups, add $-OH$ and $-C=O$ groups in the carbon chain. Because $C_{18}H_{31}NO$
455 possesses as many as 4 C=C double bonds, sequential pathway 3 and 4 reactions
456 produce a large number of oxidation products, among which 57 are found in the

457 formula list detected in 10-18 nm particles (Figure S9). These products
458 $C_{18}H_{31}NO_{4-11,13}$, $C_{18}H_{33}NO_{4,6-10}$, $C_{18}H_{35}NO_{5-9}$, $C_{18}H_{37}NO_{7-12}$ and $C_{18}H_{39}NO_{10-11}$
459 explain perfectly the presence of a series of formulas with C number = 18, DBE = 0-4
460 and a $-NH_2$ group shown in Figure 2a.

461 3.3.3. *Volatility estimation*

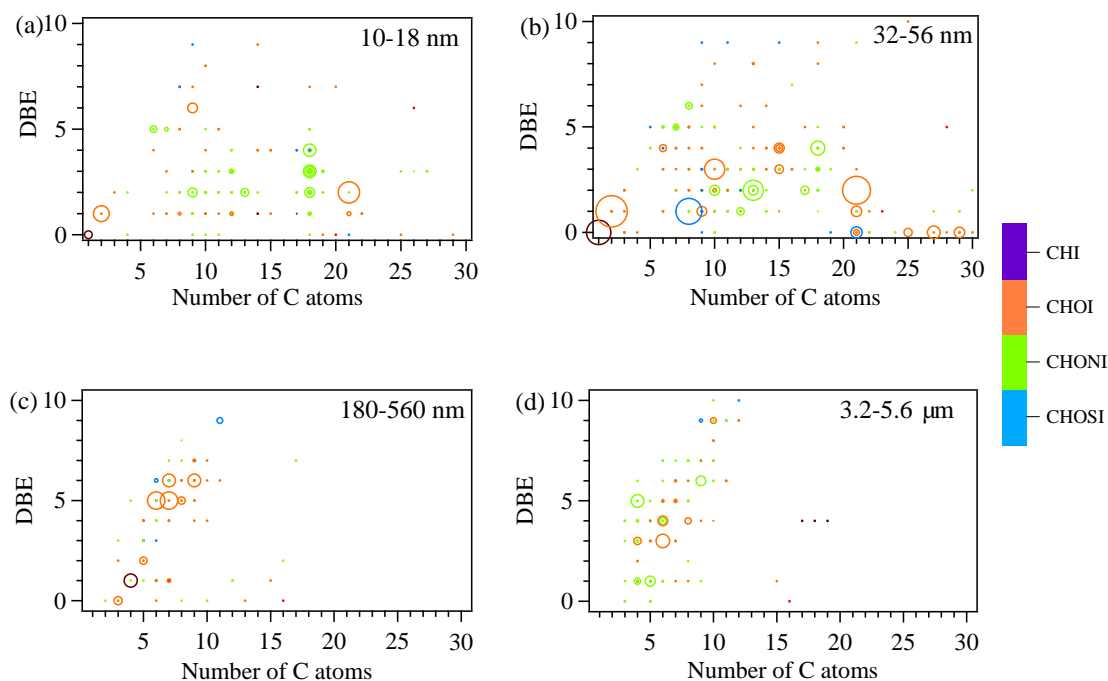
462 Based on the reaction mechanisms proposed above, it is possible to estimate the
463 volatility change from potential precursors to their oxidation products. First, from the
464 list of elemental formulas detected in 10-18 nm particles, we select 49 formulas with
465 high intensities, including 14 $CHON^-$ formulas with peak intensity $> 1.00 \times 10^8$, 23
466 $CHON^+$ formulas with peak intensity $> 3.00 \times 10^7$ and 12 CHO^- formulas (DBE = 1)
467 with peak intensities $> 3.00 \times 10^7$. Possible combinations of $-COOH$, $-ONO_2$, $-C=O$,
468 $C=C$ double bond, $-NH_2$ and $-OH$ groups are searched for every formula obeying two
469 simple rules: $CHON^-$ and CHO^- formulas must possess a carboxyl or hydroxyl group;
470 $CHON^+$ formulas must possess an amino group. Saturation concentrations (C^*) of the
471 49 formulas were then predicted for all combinations using a simple group
472 contribution method developed by Pankow and Asher (Pankow and Asher, 2008). On
473 the other hand, the C^* of their possible precursors, including unsaturated FAs, fatty
474 alcohols, nonprotein amino acids or amino alcohols, were predicted by the same
475 method.

476 As we can see in Table S4, C^* of the 49 formulas fall into the range of ELVOC ($3 \times$
477 10^{-9} - $3 \times 10^{-5} \mu g m^{-3}$) and even ULVOC (ultra-low volatility organic compound, $< 3 \times$
478 $10^{-9} \mu g m^{-3}$), while C^* of their precursors are in the range of SVOC (0.3 - $300 \mu g m^{-3}$) or
479 LVOC (3×10^{-5} - $0.3 \mu g m^{-3}$). The addition of functional groups reduces the volatility of
480 precursors by 2~7 orders of magnitude and thus make their oxidation products
481 condensable onto new particles during the I-NPF event days. According to the
482 definition of Schervish and Donahue, 2019 and Simon et al., 2020, ULVOC can even
483 drive pure biogenic nucleation. Therefore, the analysis of precursor-product volatility
484 partly supports our hypothesis about the molecular identity and formation mechanism
485 of the formulas detected in 10-18 nm particles. It should be noted that the volatility of
486 VOC oxidation products can be assessed with numerous existing parameterizations,

487 which require either exact functional groups or only the molecular formula (Peräkylä et
488 al., 2019). Their estimation can vary by up to several orders of magnitude. But this will
489 not change the conclusion drawn here.

490 3.4. Speciation of iodinated OC

491 Organic iodine compounds hold the key to understand aerosol iodine chemistry and
492 its role in regulating the recycling of halogens to the gas phase. We identified 440
493 iodinated OC formulas from the 4 size bins during the I-NPF days (Table 2). 80% of
494 the 440 formulas contain one I atom and the rest of them contain two I atoms. In
495 terms of relative intensity, iodinated OC accounts for 2.6-9.5% of OC in fine particles,
496 but its fraction in coarse particles increases to 23.3% in ESI- mode and 45% in ESI+
497 mode. The size distribution of 7 iodinated OC groups (i.e., CHOI, CHONI, CHOSI,
498 CHONSI, CHOI⁺, CHONI⁺ and CHNI⁺) resembles those of non-iodinated OC groups
499 (Figure 1). If we replace I atom(s) with H atom(s) in a formula, 107 out of 440
500 replaced formulas are also found in the non-iodine OC formula list.



501
502 Figure 4. DBE vs. C atom number diagrams of iodinated OC formulas with intensity >
503 1.00×10^7 in the four size bins. The color bar denotes the elemental groups of assigned

504 formulas. The size of the circles reflects the relative intensities of molecular formulas
505 on a logarithmic scale.

506

507 Iodinated OC with intensity $> 1.00 \times 10^7$ in the four size bins were shown in Figure 4.
508 The DBE vs. C diagram for 10-18 nm particles is characterized by (1) nine
509 $C_{18}H_hO_oN_nI$ formulas with DBE = 1-4 and (2) $C_9H_{16}NO_3I$ and its C_{10} - C_{13} homologues.
510 Because these formulas were detected in ESI+ mode, they are most likely iodinated
511 amino acids. 32-56 nm particles accommodate most abundant iodinated OC formulas,
512 in terms of both formula number and relative intensity. Prominent formulas include (1)
513 diiodo acetic acid $C_2H_2O_2I_2$, diiodomethane CH_2I_2 , (2) iodinated C_{21} carbonyls
514 $C_{21}H_{39}OI$ and $C_{21}H_{41}OI$, (3) iodinated $C_{21,25,27,29}$ alcohols or ethers with DBE = 0, (4)
515 iodinated C_{10} and C_{15} terpene and sesquiterpene oxidation products and (5) iodinated
516 organic sulfate $C_8H_{17}N_2SO_8I$ and $C_{21}H_{43}SO_4I$. In addition, $C_9H_{10}NO_3I$ detected in this
517 size bin (S/N ratio: 35) can be tentatively assigned to an iodinated amino acid
518 iodotyrosine that has been observed in seaweed (Yang et al., 2016), implying direct
519 contribution from seaweed emission to new particles.

520 In 180-560 nm particles, the majority of iodinated OC are C_{6-9} aromatic $CHOI^+$
521 compounds with AI > 0.5 and DBE = 5-7. Both C and O atom numbers of these
522 iodinated OC are smaller than those of mono-modally distributed CHO^+ compounds
523 around C_{15} in the same particle size (Figure 3d and S3b). This implies that iodine has
524 a strong tendency to aromatic compounds in submicron aerosols due to electrophilic
525 substitution on aromatic rings. In 3.2-5.6 μm particles, iodinated OC features C_4 - C_6
526 CHO^+ and $CHON^+$ compounds with DBE = 3-6, which again have fewer C atoms
527 than non-iodinated OC. Supporting evidence from AI shows these compounds are not
528 aromatic. Coastal 3.2-5.6 μm particles can be sea salt particles formed during bubble
529 bursting of sea water (Russell et al., 2010; Schmitt-Kopplin et al., 2012; Quinn et al.,
530 2014; Wilson et al., 2015). However, Hao et al. 2017 (Hao et al., 2017) showed that
531 iodinated OC products from the reaction between iodine and seawater are highly
532 unsaturated carboxylic-rich polyphenols with DBE = 4-14 and C atoms = 10-30. It is

533 thus apparent that iodinated OC in 3.2-5.6 μm particles were not directly from
534 iodinated organic compounds in the seawater.

535 **3.5 Atmospheric implications**

536 Due to the 71% ocean coverage of the earth's surface, marine aerosol generation is
537 important in determining the earth's radiative budget and climate change. Of the
538 limited number of studies reporting coastal NPF, most have focused on iodine
539 emission, oxidation and nucleation in the early stage of NPF. In principle, abundant
540 low-volatility condensing vapors other than iodine are required in coastal
541 environments for the growth of iodine clusters to CCN. This article reveals a new
542 group of important organic compounds involved in this process. It is most likely that
543 their precursors are emitted mutually with iodine from either direct exposure of
544 coastal biota to the atmosphere or biological-active sea surface. If this is true, we
545 suggest the results in our location can be extrapolated to other iodine-rich coastal
546 locations, as long as iodine-NPF can be observed. More fundamental field, laboratory
547 and modeling studies are needed to determine (1) exact emission sources and source
548 rates of these organic precursors, (2) their gas phase intermediates and oxidation
549 mechanisms in the atmosphere and (3) their quantitative contribution to global and
550 regional CCN numbers.

551 **ACKNOWLEDGMENTS**

552 The work was supported by the National Science Foundation of China (grant
553 numbers 41975831 and 41675124) and the National Key Research and Development
554 Program of China (grant number 2016YFC0203100).

555

556 ***Data availability.*** All of the datasets related to the chemical formulas detected in
557 this work can be accessed in “Global Change Research Data Publishing and
558 Repository” via doi:10.3974/geodb.2020.03.26.V1. Any other data used in this

559 publication are available from the corresponding author Huan Yu

560 (yuhuan@cug.edu.cn) upon request.

561

562 ***Author contributions.*** Huan Yu designed and conducted chemical analysis. Yibei

563 Wan and Huan Yu did data analysis and wrote the paper. Xiangpeng Huang conducted

564 the field sampling. Bin Jiang and Yuhong Liao did the FT-ICR-MS analysis. Binyu

565 Kuang, Manfei Lin, Deming Xia, Jingwen Chen and Jianzhen Yu reviewed and

566 revised the manuscript.

567

568 ***Conflict of Interest***

569 The authors declare that they have no conflict of interest.

570

571

572

573 **REFERENCE**

574 Allan, J. D., Williams, P. I., Nájera, J., Whitehead, J. D., Flynn, M. J., Taylor, J. W.,
575 Liu, D., Darbyshire, E., Carpenter, L. J., Chance, R., Andrews, S. J., Hackenberg, S.
576 C., and McFiggans, G.: Iodine observed in new particle formation events in the
577 Arctic atmosphere during ACCACIA, *Atmos. Chem. Phys.*, 15, 5599-5609,
578 doi:10.5194/acp-15-5599-2015, 2015.

579 An, Y. Q., Xu, J. Z., Feng, L., Zhang, X. H., Liu, Y. M., Kang, S. C., Jiang, B., and
580 Liao, Y. H.: Molecular characterization of organic aerosol in the Himalayas: insight
581 from ultra-high-resolution mass spectrometry, *Atmos. Chem. Phys.*, 19, 1115-1128,
582 doi:10.5194/acp-19-1115-2019, 2019.

583 Atkinson, R., Tuazon, E. C., and Aschmann, S. M.: Products of the Gas-Phase
584 Reactions of a Series of 1-Alkenes and 1-Methylcyclohexene with the OH Radical
585 in the Presence of NO, *Environ. Sci. Technol.*, 29, 1674-1680,
586 doi:10.1021/es00006a035, 1995.

587 Bao, H. Y., Niggemann, J., Li, L., Dittmar, T., and Kao, S.-J.: Molecular composition
588 and origin of water-soluble organic matter in marine aerosols in the Pacific off
589 China, *Atmos. Environ.*, 191, 27-35, doi:10.1016/j.atmosenv.2018.07.059, 2018.

590 Barnes, I., Hjorth, J., and Mihalopoulos, N.: Dimethyl Sulfide and Dimethyl Sulfoxide
591 and Their Oxidation in the Atmosphere, *Chem. Rev.*, 106, 940-975,
592 doi:10.1021/cr020529+, 2006.

593 Barone, S. B., Turnipseed, A. A., and Ravishankara, A. R.: Reaction of OH with
594 Dimethyl Sulfide (DMS). 1. Equilibrium Constant for OH + DMS Reaction and the
595 Kinetics of the OH + DMS + O₂ Reaction, *J. Phys. Chem. A.*, 100, 14694-14702,
596 doi:10.1021/jp960866k, 1996.

597 Bianco, A., Deguillaume, L., Vařilingom, M., Nicol, E., Baray, J.-L., Chaumerliac,
598 N., and Bridoux, M.: Molecular Characterization of Cloud Water Samples
599 Collected at the Puy de Dôme (France) by Fourier Transform Ion Cyclotron
600 Resonance Mass Spectrometry, *Environ. Sci. Technol.*, 52, 10275-10285,
601 doi:10.1021/acs.est.8b01964, 2018.

602 Bikkina, P., Kawamura, K., Bikkina, S., Kunwar, B., Tanaka, K., and Suzuki, K.:
603 Hydroxy Fatty Acids in Remote Marine Aerosols over the Pacific Ocean: Impact of
604 Biological Activity and Wind Speed, *ACS. Earth. Space. Chem.*, 3, 366-379,
605 doi:10.1021/acsearthspacechem.8b00161, 2019.

606 Blokker, P., Schouten, S., van den Ende, H., De Leeuw, J. W., and Sinninghe Damst é
607 J. S.: Cell wall-specific ω-hydroxy fatty acids in some freshwater green microalgae,
608 *Phytochemistry.*, 49, 691-695, doi:10.1016/S0031-9422(98)00229-5, 1998.

609 Burkholder, J. B., Curtius, J., Ravishankara, A. R., and Lovejoy, E. R.: Laboratory
610 studies of the homogeneous nucleation of iodine oxides, *Atmos. Chem. Phys.*, 4,
611 19-34, doi:10.5194/acpd-3-4943-2003, 2004.

612 Calvert, J. G., Atkinson, R. G., Orlando, J. J., Wallington, T. J., and Tyndall, G. S.:
613 The Mechanisms of Atmospheric Oxidation of Alkenes, Oxford Univ. Press,
614 Oxford, UK., 2000.

615 Cochran, R. E., Laskina, O., Trueblood, J. V., Estillore, A. D., Morris, H. S.,
616 Jayarathne, T., Sultana, C. M., Lee, C., Lin, P., Laskin, J., Laskin, A., Dowling, J.
617 A., Qin, Z., Cappa, C. D., Bertram, T. H., Tivanski, A. V., Stone, E. A., Prather, K.
618 A., and Grassian, V. H.: Molecular Diversity of Sea Spray Aerosol Particles:
619 Impact of Ocean Biology on Particle Composition and Hygroscopicity, *Chem.*
620 *Pharm. Bull.*, 2, 655-667, doi:10.1016/j.chempr.2017.03.007, 2017.

621 Crouse, J. D., Nielsen, L. B., Jørgensen, S., Kjaergaard, H. G., and Wennberg, P. O.:
622 Autoxidation of Organic Compounds in the Atmosphere, *J. Phys. Chem. Lett.*, 4,
623 3513-3520, doi:10.1021/jz4019207, 2013.

624 Daellenbach, K. R., Kourtchev, I., Vogel, A. L., Bruns, E. A., Jiang, J. H., Pet ä T.,
625 Jaffrezo, J.-L., Aksoyoglu, S., Kalberer, M., Baltensperger, U., Haddad, I. E., and
626 Prevot, A. S. H.: Impact of anthropogenic and biogenic sources on the seasonal
627 variation of the molecular composition of urban organic aerosols: a field and
628 laboratory study using ultra-high resolution mass spectrometry, *Atmos. Chem.*
629 *Phys. Discuss.*, 19, 5973-5991, doi:10.5194/acp-2018-1128, 2018.

630 Dall Osto, M., Simo, R., Harrison, R. M., Beddows, D. C. S., Saiz-Lopez, A., Lange,
631 R., Skov, H., Nøjgaard, J. K., Nielsen, I. E., and Massling, A.: Abiotic and biotic
632 sources influencing spring new particle formation in North East Greenland, *Atmos.*
633 *Environ.*, 190, 126-134, doi:10.1016/j.atmosenv.2018.07.019, 2018.

634 Dawczynski, C., Schubert, R., and Jahreis, G.: Amino acids, fatty acids, and dietary
635 fibre in edible seaweed products, *Food. Chem.*, 103, 891-899,
636 doi:10.1016/j.foodchem.2006.09.041, 2007.

637 DeMott, P. J., Mason, R. H., McCluskey, C. S., Hill, T. C. J., Perkins, R. J., Desyaterik,
638 Y., Bertram, A. K., Trueblood, J. V., Grassian, V. H., Qiu, Y., Molinero, V., Tobo,
639 Y., Sultana, C. M., Lee, C., and Prather, K. A.: Ice nucleation by particles
640 containing long-chain fatty acids of relevance to freezing by sea spray aerosols,
641 *Environ. Sci-Proc. Imp.*, 20, 1559-1569, doi:10.1039/c8em00386f, 2018.

642 Draxler, R., Rolph, G.: HYSPLIT (HYbrid Single-Particle Lagrangian Integrated
643 Trajectory) model access via NOAA ARL READY website (<http://ready.arl.noaa.gov/HYSPLIT.php>). NOAA Air Resources Laboratory. Silver Spring, MD. 25,
644 2010.

645
646 Ehn, M., Thornton, J. A., Kleist, E., Sipila, M., Junninen, H., Pullinen, I., Springer, M.,
647 Rubach, F., Tillmann, R., Lee, B., Lopez-Hilfiker, F., Andres, S., Acir, I. H.,
648 Rissanen, M., Jokinen, T., Schobesberger, S., Kangasluoma, J., Kontkanen, J.,
649 Nieminen, T., Kurten, T., Nielsen, L. B., Jorgensen, S., Kjaergaard, H. G.,
650 Canagaratna, M., Maso, M. D., Berndt, T., Petaja, T., Wahner, A., Kerminen, V. M.,
651 Kulmala, M., Worsnop, D. R., Wildt, J., and Mentel, T. F.: A large source of
652 low-volatility secondary organic aerosol, *Nature.*, 506, 476-479,
653 doi:10.1038/nature13032, 2014.

654 Elm, J., Fard, M., Bilde, M., and Mikkelsen, K. V.: Interaction of Glycine with
655 Common Atmospheric Nucleation Precursors, *J. Phys. Chem. A.*, 117,
656 12990-12997, doi:10.1021/jp408962c, 2013.

657 Ge, P., Luo, G., Luo, Y., Huang, W., Xie, H. B., Chen, J. W., and Qu, J. P.: Molecular
658 understanding of the interaction of amino acids with sulfuric acid in the presence of
659 water and the atmospheric implication, *Chemosphere.*, 210, 215-223,
660 doi:10.1016/j.chemosphere.2018.07.014, 2018.

661 Ge, X. L., Wexler, A. S., and Clegg, S. L.: Atmospheric amines – Part I. A review,
662 *Atmos. Environ.*, 45, 524-546, doi:10.1016/j.atmosenv.2010.10.012, 2011.

663 Gelin, F., Volkman, J. K., De Leeuw, J. W., and Sinninghe Damsté J. S.: Mid-chain
664 hydroxy long-chain fatty acids in microalgae from the genus *Nannochloropsis*,
665 *Phytochemistry.*, 45, 641-646, doi:10.1016/S0031-9422(97)00068-X, 1997.

666 Guo, Z. G., Sheng, L. F., Feng, J. L., and Fang, M.: Seasonal variation of solvent
667 extractable organic compounds in the aerosols in Qingdao, China, *Atmos. Environ.*,
668 37, 1825-1834, doi:10.1016/S1352-2310(03)00064-5, 2003.

669 Hao, Z. N., Yin, Y. G., Cao, D., and Liu, J. F.: Probing and Comparing the
670 Photobromination and Photoiodination of Dissolved Organic Matter by Using
671 Ultra-High-Resolution Mass Spectrometry, *Environ. Sci. Technol.*, 51, 5464-5472,
672 doi:10.1021/acs.est.6b03887, 2017.

673 Ishijima, H., Uchida, R., Ohtawa, M., Kondo, A., Nagai, K., Shima, K., Nonaka, K.,
674 Masuma, R., Iwamoto, S., Onodera, H., Nagamitsu, T., and Tomoda, H.:
675 Simplifungin and Valsafungins, Antifungal Antibiotics of Fungal Origin, *J. Org.*
676 *Chem.*, 81, 7373-7383, doi:10.1021/acs.joc.6b00952, 2016.

677 Jares-Erijman, E. A., Bapat, C. P., Lithgow-Bertelloni, A., Rinehart, K. L., and Sakai,
678 R.: Crucigasterins, new polyunsaturated amino alcohols from the mediterranean
679 tunicate *Pseudodistoma crucigaster*, *J. Org. Chem.*, 58, 5732-5737,
680 doi:10.1021/jo00073a036, 1993.

681 Jen, C. N., McMurry, P. H., and Hanson, D. R.: Stabilization of Sulfuric Acid Dimers
682 by Ammonia, Methylamine, Dimethylamine, and Trimethylamine, *J. Geophys.*
683 *Res-Atmos.*, 119, 7502-7514, doi:10.1002/2014JD021592, 2014.

684 Jiang, B., Kuang, B. Y., Liang, Y. M., Zhang, J. Y., Huang, X. H. H., Xu, C. M., Yu, J.,
685 and Shi, Q.: Molecular composition of urban organic aerosols on clear and hazy
686 days in Beijing: A comparative study using FT-ICR MS, *Environ. Chem.*, 13,
687 888-901, doi:10.1071/EN15230, 2016.

688 Kendel, M., Barnathan, G., Fleurence, J., Rabesaotra, V., and Wielgosz-Collin, G.:
689 Non-methylene Interrupted and Hydroxy Fatty Acids in Polar Lipids of the Alga
690 *Grateloupia turuturu* Over the Four Seasons, *Lipids.*, 48, 535-545,
691 doi:10.1007/s11745-013-3783-5, 2013.

692 Kim, K. R., and Oh, D. K.: Production of hydroxy fatty acids by microbial fatty
693 acid-hydroxylation enzymes, *Biotechnol. Adv.*, 31, 1473-1485,
694 doi:10.1016/j.biotechadv.2013.07.004, 2013.

695 Kourtchev, I., Fuller, S., Aalto, J., Ruuskanen, T. M., McLeod, M. W., Maenhaut, W.,
696 Jones, R., Kulmala, M., and Kalberer, M.: Molecular composition of boreal forest
697 aerosol from Hyytiala, Finland, using ultrahigh resolution mass spectrometry,
698 *Environ. Sci. Technol.*, 47, 4069-4079, doi:10.1021/es3051636, 2013.

699 Kumar, M., Saiz-Lopez, A., and Francisco, J. S.: Single-Molecule Catalysis Revealed:
700 Elucidating the Mechanistic Framework for the Formation and Growth of
701 Atmospheric Iodine Oxide Aerosols in Gas-Phase and Aqueous Surface
702 Environments, *J. Am. Chem. Soc.*, 140, 14704-14716, 10.1021/jacs.8b07441,
703 2018.

704 Kurt n, T., Loukonen, V., Vehkam ki, H., and Kulmala, M.: Amines are likely to
705 enhance neutral and ion-induced sulfuric acid-water nucleation in the atmosphere
706 more effectively than ammonia, *Atmos. Chem. Phys.*, 8, 7455-7476,
707 doi:10.5194/acpd-8-7455-2008, 2008.

708 Li, D. F., Chen, D. P., Liu, F. Y., and Wang, W. L.: Role of glycine on sulfuric
709 acid-ammonia clusters formation: Transporter or participator, *J. Environ. Sci.* , 89,
710 125-135, doi:10.1016/j.jes.2019.10.009, 2020.

711 Lin, P., Rincon, A. G., Kalberer, M., and Yu, J. Z.: Elemental Composition of HULIS
712 in the Pearl River Delta Region, China: Results Inferred from Positive and Negative
713 Electrospray High Resolution Mass Spectrometric Data, *Environ. Sci. Technol.*, 46,
714 7454-7462, doi:10.1021/es300285d, 2012.

715 Litchfield, C., Greenberg, A. J., Noto, G., and Morales, R. W.: Unusually high levels
716 of C24–C30 fatty acids in sponges of the class demospongiae, *Lipids.*, 11, 567-570,
717 doi:10.1007/BF02532903, 1976.

718 Mahajan, A. S., Sorribas, M., Mart ń, J. C. G., MacDonald, S. M., Gil, M., Plane, J. M.
719 C., and Saiz-Lopez, A.: Concurrent observations of atomic iodine, molecular iodine
720 and ultrafine particles in a coastal environment, *Atmos. Chem. Phys. Discuss.*, 11,
721 2545-2555, doi:10.5194/acp-11-2545-2011, 2010.

722 Mahajan, A. S., Plane, J. M. C., Oetjen, H., Mendes, L., Saunders, R. W., Saiz-Lopez,
723 A., Jones, C. E., Carpenter, L. J., and McFiggans, G. B.: Measurement and
724 modelling of tropospheric reactive halogen species over the tropical Atlantic Ocean,
725 *Atmos. Chem. Phys.*, 10, 4611–4624, doi: 10.5194/acp-10-4611-2010, 2010.

726 Mahajan, A. S., Martin, J. C. G., Hay, T. D., Royer, S. J., Yvon-Lewis, S., Liu, Y., Hu,
727 L., Prados-Roman, C., Ordonez, C., Plane, J. M. C., and Saiz-Lopez, A.: Latitudinal
728 distribution of reactive iodine in the Eastern Pacific and its link to open ocean
729 sources, *Atmos. Chem. Phys.*, 12, 11609-11617, 10.5194/acp-12-11609-2012,
730 2012.

731 Mansour, M. P., Volkman, J. K., Holdsworth, D. G., Jackson, A. E., and Blackburn, S.
732 I.: Very-long-chain (C28) highly unsaturated fatty acids in marine dinoflagellates,
733 *Phytochemistry.*, 50, 541-548, doi:10.1016/S0031-9422(98)00564-0, 1999.

734 Mazzoleni, L. R., Saranjampour, P., Dalbec, M. M., Samburova, V., Hallar, G. A.,
735 Zielinska, B., Lowenthal, D. H., and Kohl, S.: Identification of water-soluble
736 organic carbon in non-urban aerosols using ultrahigh-resolution FT-ICR mass
737 spectrometry: Organic anions, *Environ. Chem.*, 9, 285-297, doi:10.1071/EN11167,
738 2012.

739 Mäkel ä J. M., Hoffmann, T., Holzke, C., Väkev ä M., Suni, T., Mattila, T., Aalto, P.
740 P., Tapper, U., Kauppinen, E. I., and O'Dowd, C. D.: Biogenic iodine emissions
741 and identification of end - products in coastal ultrafine particles during nucleation
742 bursts, *J. Geophys. Res.*, 107(D19), 8110, doi:10.1029/2001JD000580, 2002.

743 Mentel, T. F., Springer, M., Ehn, M., Kleist, E., Pullinen, I., Kurt ń, T., Rissanen, M.,
744 Wahner, A., and Wildt, J.: Formation of highly oxidized multifunctional
745 compounds: autoxidation of peroxy radicals formed in the ozonolysis of alkenes –
746 deduced from structure–product relationships, *Atmos. Chem. Phys.*, 15, 6745-6765,
747 doi:10.5194/acp-15-6745-2015, 2015.

748 Merikanto, J., Spracklen, D. V., Mann, G. W., Pickering, S. J., and Carslaw, K. S.:
749 Impact of nucleation on global CCN, *Atmos. Chem. Phys.*, 9, 12999–13037,
750 doi:10.5194/acp-9-8601-2009, 2009.

751 Metzger, A., Verheggen, B., Dommen, J., Duplissy, J., Prevot, A. S. H., Weingartner,
752 E., Riipinen, I., Kulmala, M., Spracklen, D. V., Carslaw, K. S., and Baltensperger,
753 U.: Evidence for the role of organics in aerosol particle formation under
754 atmospheric conditions, *Proc. Natl. Acad. Sci. U. S. A.*, 107, 6646-6651,
755 doi:10.1073/pnas.0911330107, 2010.

756 Moss, G. P., Smith, P. A. S., and Tavernier, D.: Glossary of class names of organic
757 compounds and reactivity intermediates based on structure (IUPAC

758 Recommendations 1995), *pac*, 67, 1307-1375, doi:10.1351/pac199567081307,
759 1995.

760 Ning, C. P., Gao, Y., Zhang, H. J., Yu, H. R., Wang, L., Geng, N. B., Cao, R., and
761 Chen, J. P.: Molecular characterization of dissolved organic matters in winter
762 atmospheric fine particulate matters (PM_{2.5}) from a coastal city of northeast China,
763 *Sci. Total. Environ.*, 689, 312-321, doi:10.1016/j.scitotenv.2019.06.418, 2019.

764 O'Dowd, C. D., Jimenez, J. L., Bahreini, R., Flagan, R. C., Seinfeld, J. H., Häneri, K.,
765 Pirjola, L., Kulmala, M., Jennings, S. G., and Hoffmann, T.: Marine aerosol
766 formation from biogenic iodine emissions, *Nature.*, 417, 632-636,
767 doi:10.1038/nature00775, 2002.

768 Pankow, J. F., and Asher, W. E.: SIMPOL.1: a simple group contribution method for
769 predicting vapor pressures and enthalpies of vaporization of multifunctional
770 organic compounds, *Atmos. Chem. Phys.*, 8, 2773-2796,
771 doi:10.5194/acp-8-2773-2008, 2008.

772 Pollard, M., Beisson, F., Li, Y., and Ohlrogge, J. B.: Building lipid barriers:
773 biosynthesis of cutin and suberin, *Trends. Plant. Sci.*, 13, 236-246,
774 doi:10.1016/j.tplants.2008.03.003, 2008.

775 Peräkylä O., Riva, M., Heikkinen, L., Quđ éver, L., Roldin, P., and Ehn, M.:
776 Experimental investigation into the volatilities of highly oxygenated organic
777 molecules (HOMs) , *Atmos. Chem. Phys.*, 20, 649–669,
778 doi:10.5194/acp-2019-620, 2020.

779 Pospisilova, V., Lopez-Hilfiker, F. D., Bell, D. M., El Haddad, I., Mohr, C., Huang,
780 W., Heikkinen, L., Xiao, M., Dommen, J., Prevot, A. S. H., Baltensperger, U., &
781 Slowik, J. G.: On the fate of oxygenated organic molecules in atmospheric aerosol
782 particles. *Science Advances*, 6(11), 1–12., doi: 10.1126/sciadv.aax8922, 2020.

783 Pratt, K. A., and Prather, K. A.: Mass spectrometry of atmospheric aerosols--recent
784 developments and applications. Part I: Off-line mass spectrometry techniques,
785 *Mass. Spectrom. Rev.*, 31, 1-16, doi:10.1002/mas.20322, 2012.

786 Quinn, P. K., Bates, T. S., Schulz, K. S., Coffman, D. J., Frossard, A. A., Russell, L.
787 M., Keene, W. C., and Kieber, D. J.: Contribution of sea surface carbon pool to
788 organic matter enrichment in sea spray aerosol, *Nat. Geosci.*, 7, 228-232,
789 doi:10.1038/ngeo2092, 2014.

790 Řezanka, T., and Podojil, M.: The very long chain fatty acids of the green
791 alga, *Chlorella kessleri*, *Lipids.*, 19, 472, doi:10.1007/BF02537412, 1984.

792 Richters, S., Herrmann, H., and Berndt, T.: Highly Oxidized RO₂ Radicals and
793 Consecutive Products from the Ozonolysis of Three Sesquiterpenes, *Environ. Sci.*
794 *Technol.*, 50, 2354-2362, doi:10.1021/acs.est.5b05321, 2016.

795 Rogge, W. F., Hildemann, L. M., Mazurek, M. A., Cass, G. R., and Simoneit, B. R. T.:
796 Sources of fine organic aerosol. 1. Charbroilers and meat cooking operations,
797 *Environ. Sci. Technol.*, 25, 1112-1125, doi:10.1021/es00018a015, 1991.

798 Roscoe, H. K., Jones, A. E., Brough, N., Weller, R., Saiz-Lopez, A., Mahajan, A. S.,
799 Schoenhardt, A., Burrows, J. P., and Fleming, Z. L.: Particles and iodine
800 compounds in coastal Antarctica, *J. Geophys. Res-Atmos.*, 120, 7144-7156,
801 doi:10.1002/2015JD023301, 2015.

802 Russell, L. M., Hawkins, L. N., Frossard, A. A., Quinn, P. K., and Bates, T. S.:
803 Carbohydrate-like composition of submicron atmospheric particles and their
804 production from ocean bubble bursting, *Proc. Natl. Acad. Sci. U. S. A.*, 107, 6652,
805 doi:10.1073/pnas.0908905107, 2010.

806 Saiz-Lopez, A., and Plane, J. M. C.: Novel iodine chemistry in the marine boundary
807 layer, *Geophys. Res. Lett.*, 31, L04112, doi:10.1029/2003GL019215, 2004.

808 Saiz-Lopez, A., Plane, J. M. C., Baker, A. R., Carpenter, L. J., von Glasow, R., Gómez
809 Mart ́n, J. C., McFiggans, G., and Saunders, R. W.: Atmospheric Chemistry of
810 Iodine, *Chem. Rev.*, 112, 1773-1804, doi:10.1021/cr200029u, 2012.

811 Schervish, M., and Donahue, N. M.: Peroxy Radical Chemistry and the Volatility
812 Basis Set. *Atmos. Chem. Phys.*, 20, 1183–1199, doi: 10.5194/acp-20-1183-2020,
813 2020.

814 Schmitt-Kopplin, P., Liger-Belair, G., Koch, B. P., Flerus, R., Kattner, G., Harir, M.,
815 Kanawati, B., Lucio, M., Tziotis, D., Hertkorn, N., and Gebefügi, I.: Dissolved
816 organic matter in sea spray: a transfer study from marine surface water to aerosols,
817 *Biogeosciences.*, 9, 1571-1582, doi:10.5194/bg-9-1571-2012, 2012.

818 Schum, S. K., Zhang, B., Džepina, K., Fialho, P., Mazzoleni, C., and Mazzoleni, L. R.:
819 Molecular and physical characteristics of aerosol at a remote free troposphere site:
820 implications for atmospheric aging, *Atmos. Chem. Phys.*, 18, 14017-14036,
821 doi:10.5194/acp-18-14017-2018, 2018.

822 Simon, M., Dada, L., Heinritzi, M., Scholz, W., Stolzenburg, D., Wagner, A. C.,
823 Kürten, A., Rörup, B., He, X., Almeida, J., Baccarini, A., Bauer, P. S., Beck, L.,
824 Bergen, A., Bianchi, F. et al.: Molecular understanding of new-particle formation
825 from alpha-pinene between $-50\text{ }^{\circ}\text{C}$ and $25\text{ }^{\circ}\text{C}$, *Atmos. Chem. Phys. Discuss.*,
826 <https://doi.org/10.5194/acp-2019-1058>, in review, 2020.

827 Simoneit, B. R. T., and Mazurek, M. A.: Organic matter of the troposphere—II.**For
828 Part I, see Simoneit et al. (1977). Natural background of biogenic lipid matter in
829 aerosols over the rural western united states, *Atmos. Environ.*, 16, 2139-2159,
830 doi:10.1016/0004-6981(82)90284-0, 1982.

831 Sipil ä M., Sarnela, N., Jokinen, T., Henschel, H., Junninen, H., Kontkanen, J.,
832 Richters, S., Kangasluoma, J., Franchin, A., Per äkyl ä O., Rissanen, M. P., Ehn, M.,
833 Vehkam äki, H., Kurten, T., Berndt, T., Pet äj ä T., Worsnop, D., Ceburnis, D.,
834 Kerminen, V.-M., Kulmala, M., and O'Dowd, C.: Molecular-scale evidence of
835 aerosol particle formation via sequential addition of HIO₃, *Nature.*, 537, 532-534,
836 doi:10.1038/nature19314, 2016.

837 Stevanović, K. Z., Bubanja, I. N. M., and Stanisavljev, D. R.: Is Iodine Oxidation with
838 Hydrogen Peroxide Coupled with Nucleation Processes?, *J. Phys. Chem. C.*, 123,
839 16671-16680, doi:10.1021/acs.jpcc.9b02563, 2019.

840 Tsukamoto, D., Shibano, M., and Kusano, G.: Studies on the Constituents of
841 Broussonetia Species X. Six New Alkaloids from Broussonetia kazinoki SIEB,
842 *Chem. Pharm. Bull.*, 49, 1487-1491, doi:10.1248/cpb.49.1487, 2001.

843 Vaattovaara, P., Huttunen, P. E., Yoon, Y. J., Joutsensaari, J., Lehtinen, K. E. J.,
844 O'Dowd, C. D., and Laaksonen, A.: The composition of nucleation and Aitken
845 modes particles during coastal nucleation events: evidence for marine secondary

846 organic contribution, *Atmos. Chem. Phys.*, **6**, 4601–4616, doi:
847 10.5194/acp-6-4601-2006, 2006.

848 VanMiddlesworth, F., Giacobbe, R. A., Lopez, M., Garrity, G., Bland, J., Bartizal, K.,
849 Fromtling, R. A., Polishook, J., Zweerink, M., and Edison, A. M.: Sphingofungins
850 A, B, C, and D; a new family of antifungal agents. I. Fermentation, isolation, and
851 biological activity, *J. Antibiot.*, **45**, 861-867, 1992.

852 Vereecken, L., Glowacki, D. R., and Pilling, M. J.: Theoretical Chemical Kinetics in
853 Tropospheric Chemistry: Methodologies and Applications, *Chem. Rev.*, **115**,
854 4063-4114, doi:10.1021/cr500488p, 2015.

855 Volkman, J. K., Barrett, S. M., Dunstan, G. A., and Jeffrey, S. W.: C30-C32 alkyl
856 diols and unsaturated alcohols in microalgae of the class Eustigmatophyceae, *Org.*
857 *Geochem.*, **18**, 131-138, doi:10.1016/0146-6380(92)90150-V, 1992.

858 Wang, Y., Riva, M., Xie, H., Heikkinen, L., Schallhart, S., Zha, Q., Yan, C., He, X.,
859 Peräkylä O., and Ehn, M.: Formation of highly oxygenated organic molecules
860 from chlorine atom initiated oxidation of alpha-pinene. *Atmospheric Chemistry*
861 *and Physics*, **20**, 5145–5155. doi:10.5194/acp-2019-807, 2020.

862 Willoughby, A. S., Wozniak, A. S., and Hatcher, P. G.: Detailed Source-Specific
863 Molecular Composition of Ambient Aerosol Organic Matter Using Ultrahigh
864 Resolution Mass Spectrometry and ¹H NMR, *Atmosphere.*, **7**, 79,
865 doi:10.3390/atmos7060079, 2016.

866 Wilson, T. W., Ladino, L. A., Alpert, P. A., Breckels, M. N., Brooks, I. M., Browse, J.,
867 Burrows, S. M., Carslaw, K. S., Huffman, J. A., Judd, C., Kilthau, W. P., Mason, R.
868 H., McFiggans, G., Miller, L. A., Nájera, J. J., Polishchuk, E., Rae, S., Schiller, C.
869 L., Si, M., Temprado, J. V., Whale, T. F., Wong, J. P. S., Wurl, O.,
870 Yakobi-Hancock, J. D., Abbatt, J. P. D., Aller, J. Y., Bertram, A. K., Knopf, D. A.,
871 and Murray, B. J.: A marine biogenic source of atmospheric ice-nucleating particles,
872 *Nature.*, **525**, 234-238, doi:10.1038/nature14986, 2015.

873 Wu, C. H., Yang, J., Fu, Q., Zhu, B., Ruan, T., and Jiang, G. B.: Molecular
874 characterization of water-soluble organic compounds in PM_{2.5} using ultrahigh
875 resolution mass spectrometry, *Sci. Total. Environ.*, **668**, 917-924,
876 doi:10.1016/j.scitotenv.2019.03.031, 2019.

877 Xie, Q. R., Su, S. H., Chen, S., Xu, Y. S., Cao, D., Chen, J., Ren, L. J., Yue, S. Y.,
878 Zhao, W. Y., Sun, Y. L., Wang, Z. F., Tong, H. J., Su, H., Cheng, Y. F., Kawamura,
879 K., Jiang, G. B., Liu, C. Q., and Fu, P. Q.: Molecular Characterization of
880 Firework-Related Urban Aerosols using FT-ICR Mass Spectrometry, *Atmos. Chem.*
881 *Phys.*, **1-29**, doi: 10.5194/acp-2019-1180, 2020.

882 Yang, Y. J., Peng, Y. E., Chang, Q., Dan, C. H., Guo, W., and Wang, Y. X.: Selective
883 Identification of Organic Iodine Compounds Using Liquid Chromatography–High
884 Resolution Mass Spectrometry, *Anal. Chem.*, **88**, 1275-1280,
885 doi:10.1021/acs.analchem.5b03694, 2016.

886 Yao, L., Wang, M. Y., Wang, X. K., Liu, Y. J., Chen, H. F., Zheng, J., Nie, W., Ding,
887 A. J., Geng, F. H., Wang, D. F., Chen, J. M., Worsnop, D. R., and Wang, L.:
888 Detection of atmospheric gaseous amines and amides by a high-resolution
889 time-of-flight chemical ionization mass spectrometer with protonated ethanol

890 reagent ions, *Atmos. Chem. Phys.*, 16, 14527-14543,
891 doi:10.5194/acp-16-14527-2016, 2016.

892 Yassine, M. M., Harir, M., Dabek, E., and Schmitt-Kopplin, P.: Structural
893 characterization of organic aerosol using Fourier transform ion cyclotron resonance
894 mass spectrometry: Aromaticity equivalent approach, *Rapid. Commun. Mass. Sp.*,
895 28, 2445-2454, doi:10.1002/rcm.7038, 2014.

896 Yoon, Y. J., O'Dowd, C. D., Jennings, S. G., and Lee, S. H.: Statistical characteristics
897 and predictability of particle formation events at Mace Head, *J. Geophys. Res.*, 111,
898 D13204, doi:10.1029/2005JD006284, 2006.

899 Yu, H., Ren, L. L., Huang, X. P., Xie, M. J., He, J., and Xiao, H.: Iodine speciation and
900 size distribution in ambient aerosols at a coastal new particle formation hotspot in
901 China, *Atmos. Chem. Phys.*, 19, 4025-4039, doi:10.5194/acp-19-4025-2019, 2019.

902 Yvon, S. A., Saltzman, E. S., Cooper, D. J., Bates, T. S., and Thompson, A. M.:
903 Atmospheric sulfur cycling in the tropical Pacific marine boundary layer (12 °S,
904 135 °W): A comparison of field data and model results: 1. Dimethylsulfide, *J.*
905 *Geophys. Res.-Atmos.*, 101, 6899-6909, doi:10.1029/95JD03356, 1996.

906 Zhao, R., Kenseth, C. M., Huang, Y., Dalleska, N. F., Kuang, X. M., Chen, J.,
907 Paulson, S. E., & Seinfeld, J. H.: Rapid Aqueous-Phase Hydrolysis of Ester
908 Hydroperoxides Arising from Criegee Intermediates and Organic Acids. *Journal*
909 *of Physical Chemistry A*, 122(23), 5190–5201. doi: 10.1021/acs.jpca.8b02195,
910 2018.

911 Zhao, R.; Kenseth, C. M.; Huang, Y.; Dalleska, N. F.; Seinfeld, J. H.
912 Iodometry-assisted liquid chromatography electrospray ionization mass
913 spectrometry for analysis of organic peroxides - an application to atmospheric
914 secondary organic aerosol. *Environ. Sci. Technol.* 2018, 52, 2108–2117.

915 Zhao, Y., Hallar, A. G., and Mazzoleni, L. R.: Atmospheric organic matter in clouds:
916 exact masses and molecular formula identification using ultrahigh-resolution
917 FT-ICR mass spectrometry, *Atmos. Chem. Phys.*, 13, 12343-12362,
918 doi:10.5194/acp-13-12343-2013, 2013.

919 Zheng, M., Fang, M., Wang, F., and To, K. L.: Characterization of the solvent
920 extractable organic compounds in PM2.5 aerosols in Hong Kong, *Atmos. Environ.*,
921 34, 2691-2702, doi:10.1016/S1352-2310(99)00521-X, 2000.

922 Zuth, C., Vogel, A. L., Ockenfeld, S., Huesmann, R., and Hoffmann, T.:
923 Ultrahigh-Resolution Mass Spectrometry in Real Time: Atmospheric Pressure
924 Chemical Ionization Orbitrap Mass Spectrometry of Atmospheric Organic Aerosol,
925 *Anal. Chem.*, 90, 8816-8823, doi:10.1021/acs.analchem.8b00671, 2018.

926